Journal of Power Sources 202 (2012) 389–393

Contents lists available at SciVerse ScienceDirect

Journal of Power Sources

journal homepage: www.elsevier.com/locate/jpowsour

Short communication

Enhance electrochemical performance of lithium sulfur battery through a solution-based processing technique

Kefei Li [a], Bei Wang [a], Dawei Su [a], Jinsoo Park [b], Hyojun Ahn [b], Guoxiu Wang [a,b,*]

[a] Centre for Clean Energy Technology, School of Chemistry and Forensic Science, University of Technology, Sydney, Broadway, Sydney, NSW 2007, Australia
[b] School of Materials Science and Engineering, Gyeongsang National University, 900 Gazwa-dong, Jinju, Gyeongnam 660-701, Republic of Korea

ARTICLE INFO

Article history:
Received 22 September 2011
Received in revised form
17 November 2011
Accepted 18 November 2011
Available online 6 December 2011

Keywords:
Lithium sulfur battery
Sulfur/carbon nanocomposites
Solution processing
Dimethyl sulfoxide

ABSTRACT

Sulfur/carbon nanocomposites have been successfully prepared by a solution-based processing technique using dimethyl sulfoxide as the solvent. The as-prepared nanocomposites were characterized by X-ray diffraction and field emission scanning electron microscopy. The electrochemical performance of sulfur/carbon nanocomposites were tested by cyclic voltammetry and galvanostatic charge/discharge cycling. When applied as the cathode material in lithium sulfur batteries, the as-prepared sulfur/carbon nanocomposites exhibited a high reversible capacity of 1220 mAh g^{-1} in the first cycle and maintained a satisfactory cyclability. This drastic improvement of specific capacity and cycling performance could be attributed to the reduced particle size of sulfur and the homogeneous distribution of sulfur nanoparticles on a carbon matrix, resulting from this novel solution-based processing technique.

1. Introduction

Lithium ion batteries are currently the predominant power sources for portable electronic devices. However, there are tremendous challenges facing applications of lithium ion batteries such as electric vehicles and stationary energy storage for smart electricity grids because of their high cost, safety concerns and limited service life [1]. Lithium sulfur batteries are able to meet the requirements of large-scale applications owing to their high specific capacity, abundance of source materials in nature and the low cost of sulfur. Lithium sulfur batteries operate quite differently from lithium ion batteries. The overall reaction between lithium and sulfur can be expressed as:

$$16Li^+ + S_8 \leftrightarrow 8Li_2S \quad (1)$$

Based on the above complete reaction, sulfur cathode can offer a theoretical specific capacity of 1675 mAh g^{-1} and a theoretical energy density of 2600 Wh kg^{-1}, which is the second highest among all the investigated cathode materials [2,3]. The actual lithiation process proceeds as two steps with two distinguished voltage plateaus:

$$xLi^+ + S_8 + e^- \rightarrow Li_2S_x\,(2.4\,V - 2.1\,V) \quad (2)$$

$$Li_2S_x + Li^+ + e^- \rightarrow Li_2S_2 \text{ or } Li_2S\,(2.1\,V - 1.5\,V) \quad (3)$$

Sulfur is electronically and ionically insulting in nature, resulting in some serious issues like low material utilization of sulfur and low rate capacity. High solubility of polysulfide in the organic electrolyte causes capacity fading and short cycle life [4–8]. Many approaches have been investigated to overcome the above-mentioned problems. These include: (i) the addition of conductive additives (e.g. porous active carbon, carbon nanotubes, conductive polymers) in sulfur cathodes [9–19], (ii) selection of a proper solvent for electrolyte [20–25], (iii) employment of solid-state polymer electrolyte or ionic liquid electrolyte [26–31], and (iv) surface modification of electrodes [32,33]. Carbon based materials are commonly used as conductive additives for sulfur electrodes. The carbon matrix provides an electron transport network as well as reaction sites for sulfur. Many previously reported processes involved a series of complicated physical and chemical methods with prolonged preparation time and the consumption of expensive materials such as single walled carbon nanotubes, multiwalled carbon nanotubes and Nafion. A low cost and highly efficient solution processing method to prepare sulfur composites has yet to be discovered.

In this study, we have developed an innovative solution processing method to prepare conductive sulfur/carbon nanocomposites for the first time. Dimethyl sulfoxide (DMSO) was used as the solvent to dissolve sulfur. DMSO is a solvent with a high boiling point of 189 °C and a high freezing point of 18.5 °C. The solubility of sulfur in DMSO is relatively high at temperatures above 115 °C and the precipitation of sulfur is rapid when the temperature drops below 80 °C. Therefore, DMSO can be used as an efficient solvent for the preparation of sulfur/carbon nanocomposites. This

* Corresponding author. Tel.: +61 2 95141741; fax: +61 2 95141460.
E-mail address: Guoxiu.Wang@uts.edu.au (G. Wang).

0378-7753/$ – see front matter © 2011 Elsevier B.V. All rights reserved.
doi:10.1016/j.jpowsour.2011.11.073

approach is based on the different solubilities of sulfur in DMSO at different temperatures. The as-prepared sulfur/carbon nanocomposites exhibited a high reversible capacity of 1220 mAh g^{-1} and an enhanced cycling performance.

2. Experimental

2.1. Material preparation and characterization

Sulfur (Sigma Aldrich) and VX-72 Vulcan carbon powders were weighed separately in a weight ratio of 7:3 prior to the preparation of sulfur/carbon nanocomposites. In the first step, sulfur powders were dissolved in DMSO by a high-energy ultrasonic probe in a pulse mode with the temperature limit of 160 °C (Branson S-450D sonifier). Next, VX-72 carbon powders were added to the solution and dispersed by an ultrasonic probe. The mixture was stirred and cooled to room temperature, during which sulfur re-crystallized and formed sulfur/carbon nanocomposites. After that, nanocomposites were washed with ethanol and distilled water several times to eliminate the residual DMSO, then dried in a vacuum oven at 100 °C to evaporate moisture. The schematic of the preparation process is shown in Fig. 1. For the comparison, pure sulfur powders (without carbon) were also prepared by the above solution-based processing. X-ray diffraction (XRD, Siemens D5000 X-ray diffractometer) and thermo-gravimetric analysis (TGA, TA Instruments, SDT 2960 module) were carried out to examine the sulfur imbibitions and weight percentage of sulfur in nanocomposites. Field emission scanning electron microscopy analysis (FESEM) was performed to investigate the morphology and back-scattered electron image of sulfur/carbon nanocomposites (Zeiss Supra 55VP FESEM with an Oxford EDS system).

2.2. Electrode fabrication and electrochemical testing

Sulfur/carbon nanocomposites, poly (vinylidene fluride) binder and carbon black with a weight ratio of 80:10:10 were mixed in N-methyl-2-pyrrolidinone solvent. The slurry was then coated on the aluminum foil and dried under vacuum at 80 °C for 12 h. Electrodes were punched into round disks with a diameter of 14 mm. CR2032 coin cells were assembled in an argon-filled glove box with both O_2 and H_2O level less than 0.1 ppm (UniLab, Mbraun, Germany). 1 M lithium bis(trifluoromethane sulfonyl)imide ($LiN(SO_2CF_3)_2$, LiTFSI) in 1,2-dimethoxyethane and 1,3-dioxolane (4:1 by volume) solution was prepared and used as the electrolyte. The charge/discharge cycling tests were performed on a Neware RS-232 battery test system in galvanostatic mode with cut-off voltages of 1.0 V and 3.0 V. Cyclic voltammetry (CV) and A.C. impedance measurements were conducted with a CHI CJ660D electrochemical workstation using fresh cells at open potential. The CV measurement was performed at a scanning rate of 0.1 mV s^{-1}. A.C. impedance spectra were measured at ±5 mV amplitude with a frequency range from 0.01 Hz to 100 kHz.

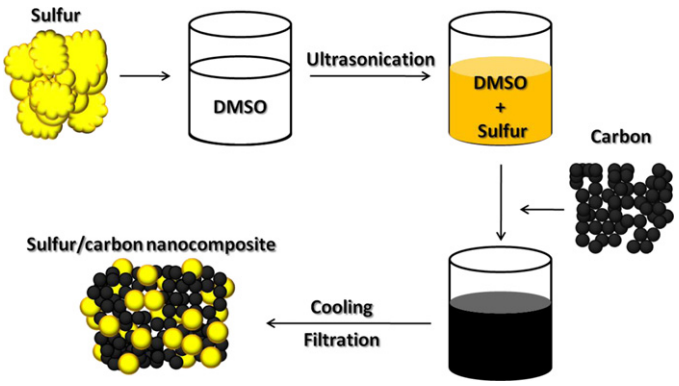

Fig. 1. Schematic of the solution processing for the preparation of sulfur/carbon nanocomposites.

3. Results and discussion

Fig. 2(a) and (b) shows the XRD patterns of the pristine sulfur powders and the as-prepared sulfur/carbon nanocomposites, respectively. All diffraction peaks of sulfur match very well with the standard diffraction lines of sulfur (JCPDS card No. 08-0247), which can be indexed to the orthorhombic phase with the space group of Fddd. For sulfur/carbon nanocomposites, the XRD pattern consists of diffraction peaks of sulfur and a broad diffraction peak at 25°, which corresponds to amorphous carbon in the composite. This indicates that sulfur re-crystallized after the solution-based processing by DMSO. The morphology and distribution of sulfur in the as-prepared sulfur/carbon nanocomposites were analyzed by FESEM. The pristine sulfur particles are polycrystalline particles with particle sizes in the range of a few tens of micrometers (as shown in Fig. 3(a)). Pure sulfur was also prepared by the solution-based processing using dimethyl sulfoxide (DMSO) as the solvent.

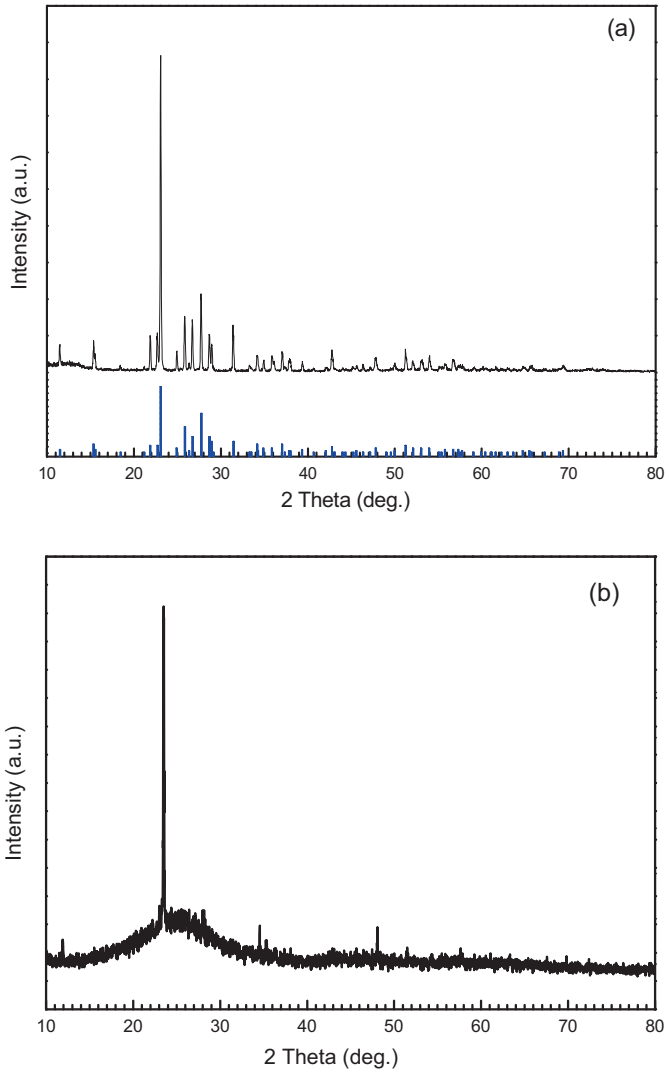

Fig. 2. X-ray diffraction pattern (a) pure sulfur powders, (b) sulfur/carbon nanocomposites. The standard diffraction pattern of sulfur is presented on the bottom in (a).

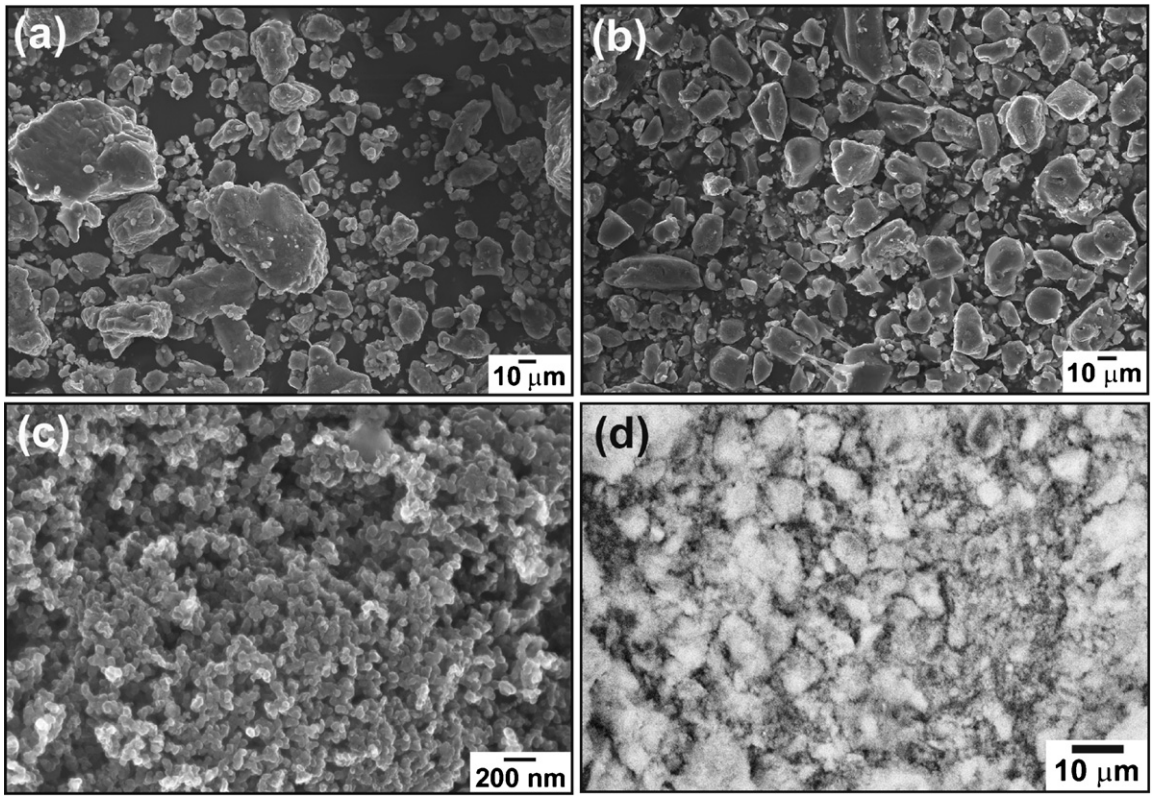

Fig. 3. FESEM images of (a) pristine sulfur powders, (b) DMSO processed sulfur powders, (c) sulfur/carbon nanocomposites, and (d) back-scattered electron image of S/C nanocomposites.

As shown in Fig. 3(c), the particle size of the DMSO processed sulfur is in the range of micrometer size, which is similar to the pristine sulfur powders. A FESEM image of sulfur/carbon nanocomposites is shown in Fig. 3(b), from which the mixture of super-fine nanocomposite particles can be clearly identified. During the dissolution processing, sulfur was dissolved by the solvent DMSO and intimately mixed with carbon matrix. During the cooling process, sulfur re-crystallized from the solution and is expected to homogeneously distribute on carbon matrix. The crystal size of sulfur has been significantly reduced to a range of a few tens to a hundred nanometers after this dissolution and re-crystallization process. Fig. 3(d) shows the back-scattered electron image of S/C nanocomposites at a low magnification, from which the uniform distribution of sulfur in carbon matrix can be seen. The light (white) color represents sulfur element, which is mixed well with carbon (dark color). Therefore, the solution-based processing can allow the formation of sulfur/carbon nanocomposites containing crystalline sulfur with a significantly reduced particle size of sulfur. The content of sulfur in S/C nanocomposites was determined by thermal gravimetric analysis (TGA). Fig. 4 shows the TGA curve of the as-prepared sulfur/carbon nanocomposites. The nanocomposites contains 64.74 wt% sulfur, which is slightly lower than the nominal value (70 wt%). Apparently, small amounts of sulfur did not re-crystallize after being dissolved in DMSO solvent.

Fig. 5 shows the cyclic voltammetry (CV) curves of the sulfur/carbon nanocomposite electrode in the voltage window of 1.0–3.0 V. As Vulcan carbon is electrochemically inert in this voltage range, the redox peaks can only be ascribed to the redox reactions associated with sulfur and lithium ions. In the first cycle, two cathodic peaks are identified, which can be assigned to the reduction processes of sulfur. The first cathodic peak at around 2.2 V corresponds to the reduction of elemental sulfur to polysulfide. As the reduction proceeded, lithium polysulfides were reduced to lithium sulfides, which should be responsible for the second cathodic peak at 1.94 V. The anodic peak was found at 2.5 V, representing a reversible process from lithium sulfides to elemental sulfur. From the second cycle, the two reduction peaks shifted to 2.3 V and 2.0 V, respectively and the oxidation peak shifted slightly to a higher potential. The reversibility of the CV curves was improved gradually, implying enhanced sulfur utilization in the electrodes. Fig. 6 displays the charge/discharge profiles of sulfur/carbon nanocomposite electrodes in their second cycles at different current densities. Two discharge plateaus can be easily distinguished in the voltage ranges of 2.4–2.1 V and 2.1–1.5 V,

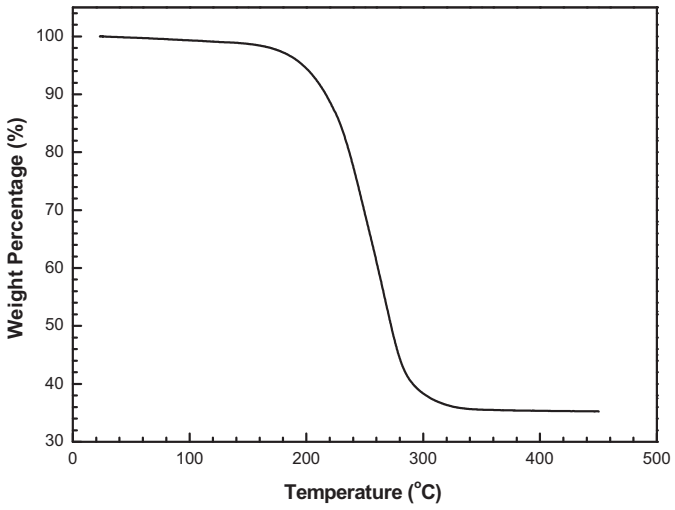

Fig. 4. TGA analysis curve of sulfur/carbon nanocomposites.

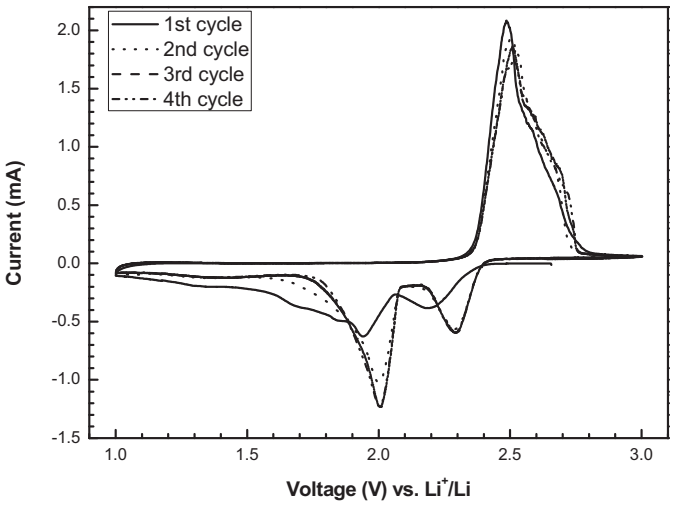

Fig. 5. Cyclic voltammetry curves of the sulfur/carbon nanocomposite electrode in the 1st, 2nd, 3rd, and 4th cycles. The scanning rate is 0.1 mV s^{-1}.

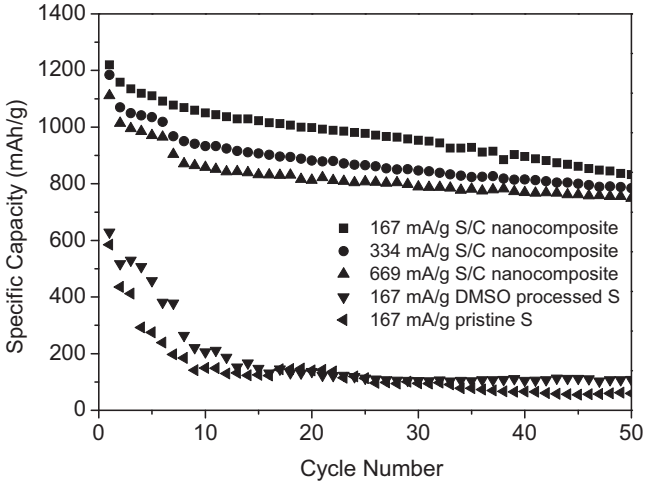

Fig. 7. Cycling performance of sulfur/carbon nanocomposite electrodes at different current densities. As a comparison, the cycling properties of the pristine sulfur electrode and the DMSO processed sulfur electrode are also presented.

respectively. The first discharge plateau is relatively shorter, while the second one extends longer and contributes to the majority of the discharge capacity. These two discharge plateaus match very well with two cathodic peaks in the CV curves (as shown in Fig. 5). The second discharge stages present a long horizontal plateau, which implies a highly complete reduction process from polysulfides to sulfides [4]. Fig. 7 shows the charge/discharge cycling performance of sulfur/carbon nanocomposite electrodes at 167 mAh g^{-1} (0.1 C), 334 mAh g^{-1} (0.2 C) and 669 mAh g^{-1} (0.4 C), respectively. The as-prepared sulfur/carbon nanocomposite delivered the highest specific discharge capacity of 1220 mAh g^{-1} at 0.1 C in the first cycle. The capacity then slightly declined on cycling, but was maintained quite well over 50 cycles. A specific capacity of 832 mAh g^{-1} was retained in the 50th cycle. The sulfur/carbon nanocomposite electrodes also achieved the maximum discharge capacities of 1184 mAh g^{-1} at 0.2 C and 1111 mAh g^{-1} at 0.4 C, with the capacity retention of 784 mAh g^{-1} and 749 mAh g^{-1}, respectively. This demonstrates an enhanced cyclability of the as-prepared nanocomposites at different current rates [16,34]. As a comparison, the cycling properties of the pristine sulfur electrode and the DMSO processed sulfur electrode are also presented in Fig. 7, which shows very poor cyclability. The continuous decrease of the capacity revealed the lack of strong combination between carbon and sulfur particles within the nanocomposite. The solution process can lead a reduced particle size of sulfur and well-distributed sulfur in carbon matrix, but cannot strongly hold sulfur on carbon. The volume expansion and contraction of sulfur during cycling could degrade the connections between carbon and sulfur, inducing the gradual decrease of capacity. On the other hand, the use of mesoporous carbon in the previous reports can effectively hold sulfur in mesopores, and therefore can achieve higher capacity and better cyclability [13,35].

Fig. 8 displays the electrochemical impedance spectroscopy (EIS) of the sulfur/carbon nanocomposite electrode and the pristine sulfur electrode, respectively. In the high frequency region, the impedance response displays a semicircle loop and the corresponding diameter represents the charge transfer resistance at the electrode/electrolyte interface. From Fig. 8, it is evident that the sulfur/carbon nanocomposite electrode demonstrates a much lower charge transfer resistance than that of the pristine sulfur electrode. This effect confirms that the nanocomposite architecture significantly increased the charge transfer process in the electrode, and therefore, improved the electrochemical performance of the lithium/sulfur batteries.

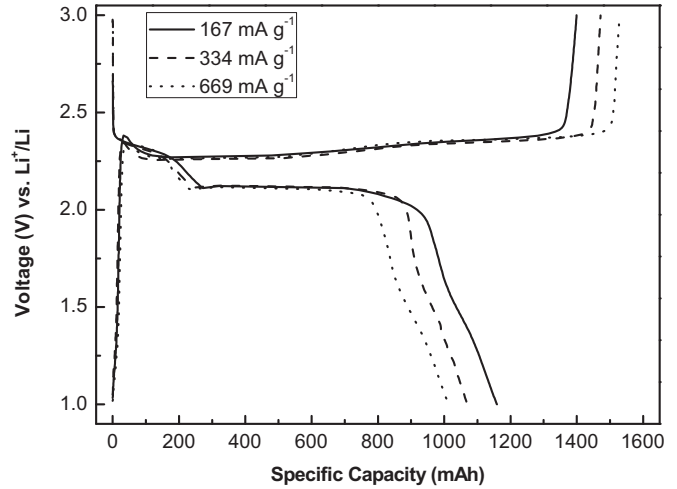

Fig. 6. The charge/discharge profiles of sulfur/carbon nanocomposite electrodes at different current densities.

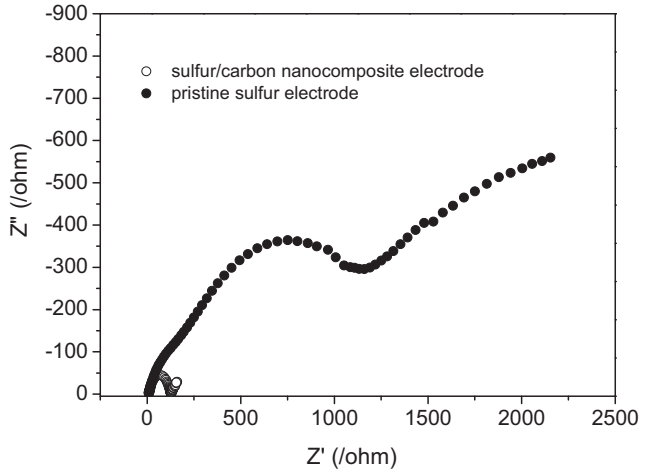

Fig. 8. A.C. impedance spectra of the pristine sulfur electrode and the sulfur/carbon nanocomposite electrode.

4. Conclusions

A solution-based processing technique has been discovered for the preparation of sulfur/carbon nanocomposites, which involves the dissolution and re-crystallization of sulfur. This technique can significantly reduce the particle size of sulfur and generate homogeneous distribution of sulfur in carbon matrix. The as-prepared sulfur/carbon nanocomposites demonstrated a high specific capacity of 1220 mAh g^{-1} at a 0.1 C rate, an enhanced cycling performance and a satisfactory high rate capacity. We expect that this approach can also be applied to prepare other sulfur containing nanocomposites such as in carbon nanotubes, graphene and mesoporous carbon matrices.

References

[1] Z. Yang, J. Zhang, M.C. Kintner-Meyer, X. Lu, D. Choi, J.P. Lemmon, J. Liu, Chem. Rev. 5 (2011) 3577–3613.
[2] B. Scrosati, J. Garche, J. Power Sources 195 (2010) 2419–2430.
[3] A. Manthiram, J. Phys. Chem. Lett. 2 (2011) 176–184.
[4] E. Peled, A. Gorenshtein, M. Segal, Y. Sternberg, J. Power Sources 26 (1989) 269–271.
[5] S.E. Cheon, K.S. Ko, J.H. Cho, S.W. Kim, E.Y. Chin, H.T. Kim, J. Electrochem. Soc. A 150 (2003) 796–799.
[6] V.S. Kolosnitsyn, E.V. Karaseva, N.A. Amineva, G.A. Batyrshina, Russ. J. Electrochem. 38 (2002) 329–331.
[7] V.S. Kolosnitsyn, E.V. Karaseva, A.L. Ivanov, Russ. J. Electrochem. 44 (2008) 564–569.
[8] X.M. He, W.H. Pu, J.G. Ren, L. Wang, J.L. Wang, C.Y. Jiang, C.R. Wan, Electrochim. Acta 52 (2007) 7372–7376.
[9] W. Wei, J.L Wang, L.J. Zhou, J. Yang, B. Schumann, Y. NuLi, Electrochem. Commun. 13 (2011) 399–402.
[10] L.X. Yuan, H.P. Yuan, X.P. Qiu, L.Q. Chen, W.T. Zhu, J. Power Sources 189 (2009) 1141–1146.
[11] W. Zheng, Y.W. Liu, X.G. Hua, C.F. Zhang, Electrochim. Acta 51 (2006) 1330–1335.
[12] J.J. Chen, X.Jia, Q.J. She, C. Wang, Q. Zhang, M.S. Zheng, Q.F. Dong, Electrochim. Acta 55 (2010) 8062–8066.
[13] X.L. Ji, K.T. Lee, L.F. Nazar, Nat. Mater. 8 (2009) 500–506.
[14] C. Liang, N.J. Dudney, J.Y. Howe, Chem. Mater. 21 (2009) 4724–4730.
[15] L. Qiu, S. Zhang, L. Zhang, M. Sun, W. Wang, Electrochim. Acta 55 (2010) 4632–4636.
[16] M.M. Sun, S.C. Zhang, T. Jiang, L. Zhang, J.H. Yu, Electrochem. Commun. 10 (2008) 1819–1822.
[17] C. Wang, J.J. Chen, Y.N. Shi, M.S. Zheng, Q.F. Dong, Electrochim. Acta 55 (2010) 7010–7015.
[18] X.G Yu, J.Y. Xie, Y. Li, H.J. Huang, C.Y. Lai, K.Wang, J. Power Sources 146 (2005) 335–339.
[19] Y.L. Cao, X.L. Li, I.A. Aksay, J. Lemmon, Z.M. Ni, Z.G. Yan, J. Liu, Phys. Chem. Chem. Phys. 13 (2011) 7660–7665.
[20] O.V. Karlova, I.A. Kedrinskii, E.A. Chudinov, M.V. Yakovleva, Russ. J. App. Chem. 79 (2006) 1952–1956.
[21] S.Kim, Y. Jung, H. Lim, Electrochim. Acta 50 (2004) 889–892.
[22] J.W. Choi, G. Cheruvallya, D.S. Kim, J.H. Ahn, K.W. Kim, H.J. Ahn, J. Power Sources 183 (2008) 441–445.
[23] W.K. Wang, Y. Wang, Y.Q. Huang, C.J. Huang, Z.B. Yu, H. Zhang, A.B. Wang, K.G. Yuan, J. Appl. Electrochem. 40 (2010) 321–325.
[24] D.R. Chang, S.H. Lee, S.W. Kima, H.T. Kim, J. Power Sources 112 (2002) 452–460.
[25] J.H. Shin, E.J. Cairns, J. Power Sources 177 (2008) 537–545.
[26] D. Marmorstein, T.H. Yu, K.A. Striebel, F.R. McLarnon, J. Hou, E.J. Cairns, J. Power Sources 89 (2000) 219–226.
[27] J.H. Shin, S.S. Jung, K.W. Kim, H.J. Ahn, J.H. Ahn, J. Mater. Sci. Mater. Electron. 13 (2002) 727–733.
[28] J.H. Shin, K.W. Kim, H.J. Ahn, J.H. Ahn, Mater. Sci. Eng. B 95 (2002) 148–156.
[29] J. Hassoun, B. Scrosati, Angew. Chem. Int. Ed. 49 (2010) 2371–2374.
[30] L.X. Yuan, J.K. Feng, X.P. Ai, Y.L. Cao, S.L. Chen, H.X. Yang, Electrochem. Commun. 8 (2006) 610–614.
[31] J. Wang, S.Y. Chew, Z.W. Zhao, S. Ashraf, D. Wexler, J. Chen, S.H. Ng, S.L. Chou, H.K. Liu, Carbon 46 (2008) 229–235.
[32] Y. Yang, M.T. McDowell, A. Jackson, J.J. Cha, S.S. Hong, Y. Cui, Nano Lett. 10 (2010) 1486–1491.
[33] Y.M. Lee, N.S. Choi, J.H. Park, J.K. Park, J. Power Sources 119 (2003) 964–972.
[34] B. Zhang, C. Lai, Z. Zhou, X.P. Gao, Electrochim. Acta 54 (2009) 3708–3713.
[35] N. Jayaprakash, J. Shen, S.S. Moganty, A. Corona, L.A. Archer, Angew. Chem. Int. Ed. 50 (2011) 5904–5908.